HHS Public Access

Author manuscript

J Cell Physiol. Author manuscript; available in PMC 2021 July 01.

Published in final edited form as:

J Cell Physiol. 2020 July ; 235(7-8): 5679–5688. doi:10.1002/jcp.29500.

Sclerostin Antibody Treatment Rescues the Osteopenic Bone Phenotype of TGFß Inducible Early Gene-1 Knockout Female Mice

Anne Gingery[1,2], **Malayannan Subramaniam**[2], **Kevin S. Pitel**[2], **Xiaodong Li**[3], **Hua Z. Ke**[4], **Russell T. Turner**[5], **Urszula T. Iwaniec**[5], **John R. Hawse**[2,*]

[1]Department of Orthopedics, Mayo Clinic, Rochester, MN, USA.

[2]Department of Biochemistry and Molecular Biology, Mayo Clinic, Rochester, MN, USA.

[3]Dept. of Metabolic Disorders, Amgen, Inc., Thousand Oaks, CA, USA.

[4]UCB Pharma, Slough, UK

[5]Skeletal Biology Laboratory, School of Biological and Population Health Sciences, Oregon State University, Corvallis, OR, USA.

Abstract

Deletion of TGFβ Inducible Early Gene-1 (TIEG) in mice results in an osteopenic phenotype which exists only in female animals. Molecular analyses on female TIEG knockout (KO) mouse bones identified increased expression of sclerostin, an effect that was confirmed at the protein level in serum. Sclerostin antibody (Scl-Ab) therapy has been shown to elicit bone beneficial effects in multiple animal model systems and human clinical trials. For these reasons, we hypothesized that Scl-Ab therapy would reverse the low bone mass phenotype of female TIEG KO mice. In this study, wildtype (WT) and TIEG KO female mice were randomized to either vehicle control (Veh, n=12/group) or Scl-Ab therapy (10 mg/kg, 1×/wk, s.c.; n=12/group) and treated for 6 weeks. Following treatment, bone imaging analyses revealed that Scl-Ab therapy significantly increased cancellous and cortical bone in the femur of both WT and TIEG KO mice. Similar effects also occurred in the vertebra of both WT and TIEG KO animals. Additionally, histomorphometric analyses revealed that Scl-Ab therapy resulted in increased osteoblast perimeter/bone perimeter in both WT and TIEG KO animals, with a concomitant increase in P1NP, a serum marker of bone formation. In contrast, osteoclast perimeter/bone perimeter and CTX1 serum levels were unaffected by Scl-Ab therapy, irrespective of mouse genotype. Overall,

* Correspondence: John R. Hawse, PhD, Department of Biochemistry and Molecular Biology, Mayo Clinic, 13–21B Guggenheim Building, 200 First St. SW, Rochester, MN 55905., hawse.john@mayo.edu.

Authors Contribution:

Study design: AG, MS, UTI, RTT, JRH; Study conduct: AG, MS, UTI, RTT, KSP, JRH; Drafting manuscript: AG. Revising manuscript: AG, MS, UTI, RTT, KSP, XL, HZK, TSC, JRH. Approving final version of manuscript: all authors. AG, MS and JRH take responsibility for the integrity of the data analysis.

Conflicts of Interest:

The authors declare no conflicts of interest.

Data Availability Statement:

The data that support the findings of this study are available from the corresponding author upon reasonable request.

our findings demonstrate that Scl-Ab therapy elicits potent bone forming effects in both WT and TIEG KO mice and effectively increases bone mass in female TIEG KO mice.

Keywords

Sclerostin; Bone; TGFβ Inducible Early Gene-1 (TIEG); Krüppel-Like Transcription Factor 10 (KLF10); Osteoporosis

1. INTRODUCTION

TGFβ Inducible Early Gene-1 (TIEG), also known as KLF10, was originally cloned from human osteoblasts by our laboratory (Subramaniam et al., 1995). TIEG is a member of the family of Krüppel-like zinc finger transcription factors and plays an important role in bone homeostasis (Bensamoun et al., 2006b; Hawse, 2008; Hawse et al., 2011; Hawse et al., 2014; Subramaniam et al., 2005; Subramaniam et al., 1995; Subramaniam et al., 2016). TIEG mis-regulation and mutation is known to be correlated with human bone disorders such as osteoporosis (Hopwood et al., 2009; Yerges et al., 2010). TIEG knockout (KO) mice exhibit a female-specific low bone mass phenotype characterized by reduced bone mineral density, content and area as well as decreased osteoblast number, impaired osteoclast differentiation, and decreased mechanical properties (Bensamoun et al., 2006a; Cicek et al., 2011; Hawse et al., 2008a; Reinholz et al., 2004; Subramaniam et al., 2005). Furthermore, TIEG plays an important role in mediating estrogen action in bone (Hawse et al., 2014; Hawse et al., 2008b).

Gene expression profiling of calvarial osteoblasts isolated from wild-type (WT) and TIEG KO mice revealed significant alterations in the expression levels of multiple Wnt pathway genes during the course of differentiation *in vitro* (Subramaniam et al., 2017a). Loss of TIEG expression was also shown to impair nuclear localization of β-catenin resulting in suppression of canonical Wnt pathway activity (Subramaniam et al., 2017a). Furthermore, increased expression of sclerostin mRNA was detected by RNAseq and RT-PCR in the cortical shells of long bones isolated from female TIEG KO mice compared to WT littermates (Subramaniam et al., 2018). Elevated circulating levels of sclerostin protein were also found in the serum of TIEG KO animals (Subramaniam et al., 2018). Further, TIEG was shown to directly suppress the activity of the SOST promoter(Subramaniam et al., 2018).

Sclerostin is a glycoprotein that inhibits Wnt/ß-catenin signaling (Hoeppner et al., 2009; Leupin et al., 2011; Li et al., 2005). Sclerostin is primarily secreted by osteocytes and is regulated by multiple factors including skeletal loading, age, hormones and cytokines (Modder et al., 2011; Robling et al., 2008). Sclerostin interferes with the extracellular Wnt receptors including lipoprotein receptor-related protein-4 (LRP4), LRP5 and LRP6 (Burgers and Williams, 2013; Canalis, 2013; Dallas et al., 2013), resulting in blockade of Wnt signaling. This inhibition of Wnt signaling results in decreased bone formation and ultimately bone loss over time. Previous work has shown that treatment with sclerostin antibodies (Scl-Ab) results in increased bone formation, decreased bone resorption and improved bone mass and quality in preclinical models of osteoporosis (Ominsky et al., 2017).

Given that female TIEG KO mice exhibit a low bone mass phenotype (Bensamoun et al., 2006a; Hawse, 2008) and have elevated levels of sclerostin (Subramaniam et al., 2018) we anticipated that Scl-Ab treatment would positively influence bone mass in this model. In this study, we provide evidence that Scl-Ab therapy increases bone mass in female TIEG KO as well as WT animals. Scl-Ab therapy resulted in significant increases in cortical and cancellous bone in the femur and lumbar vertebra. Further, Scl-Ab treatment resulted in increased bone formation and osteoblast perimeter, with no change in osteoclast perimeter or resorption markers. These data confirm an important role for TIEG in regulating canonical Wnt signaling and demonstrate that therapies which enhance Wnt pathway activity are capable of rescuing the low bone mass phenotype of female TIEG KO mice.

2. METHODS

2.1 Animals and experimental design

The WT and TIEG KO mice used in this study were developed as previously described (Subramaniam et al., 2005) and the genetic background of these mice was as previously reported (Subramaniam et al., 2017b). Nine week old female WT and TIEG KO mice were randomized to receive treatment with either 1x PBS vehicle (Veh) or Scl-Ab (10 mg/kg) (Amgen Inc, Thousand Oaks, CA; UCB, Brussels, Belgium). Twelve mice were included for each treatment group. All treatments were administered via subcutaneous injection once weekly for a total of 6 weeks. Calcein (10 mg/kg) was injected subcutaneously 4 days and 1 day before sacrifice. Animals were housed in a temperature controlled room (22 ± 2°C) with a light/dark cycle of 12 hours and had free access to water and standard laboratory chow. This protocol was approved by the Mayo Clinic Institutional Animal Care and Use Committee (Permit Number: A9615).

2.2 DXA and pQCT analyses

Following 6 weeks of treatment, mice underwent DXA scans with a Lunar PIXImus densitometer (software version 2.10) as previously described (Hawse, 2008). Bone mineral density (BMD, g/cm^2) and bone mineral content (BMC, g) were determined. pQCT scans of the tibial metaphysis and the tibial diaphysis were performed as previously described (Hawse, 2008). Total content (mg), density (mg/cm^3) as well as trabecular and cortical content (mg), density (mg/cm^3) and area (mm^2) were determined. Additionally cortical thickness (mm), as well as periosteal and endocortical circumference (mm), were analyzed.

2.3 Microcomputed Tomography (μCT)

Micro-CT was performed on the left femora and 3rd lumbar vertebrae (LV3) of each mouse following overnight fixation with 10% neutral buffered formalin. μCT was completed as previously described (Lee et al., 2017; Philbrick et al., 2015). Briefly, femora were scanned using a Scanco μCT40 scanner (Scanco Medical AG, Basserdorf, Switzerland) at a voxel size of 12 × 12 × 12 μm (55 kVp x-ray voltage, 145 μA intensity, and 200 ms integration time). Total femora (cancellous + cortical bone) were evaluated followed by analysis of cortical bone in the mid femur diaphysis and cancellous bone in the distal femur metaphysis. For the femoral diaphysis, 20 consecutive slices (240 μm) of bone were evaluated and cross-sectional volume (cortical and marrow volume, mm^3), cortical volume (mm^3), marrow

volume (mm^3), and cortical thickness (μm) were measured. For the femoral metaphysis, 42 consecutive slices (504 μm) of cancellous bone, and 75 slices (1,050 μm) proximal to the growth plate, were evaluated. For the vertebra, the region of interest was located between the cranial and caudal growth plates (151 ± 2 slices, 1,812 ± 24 μm). Direct cancellous bone measurements included cancellous bone volume fraction (bone volume/tissue volume, BV/TV, %), connectivity density (mm^{-3}), trabecular number (mm^{-1}), trabecular thickness (μm) and trabecular spacing (μm).

2.4 Histomorphometry

Histomorphometry was completed as previously described (Iwaniec et al., 2008; Lee et al., 2017). In brief, distal femora were dehydrated, embedded undecalcified, and sectioned longitudinally. One section/animal was left unstained for assessment of fluorochrome labels. Another section was stained for tartrate resistant acid phosphatase (TRAP) for assessment of osteoblast and osteoclast measurements. The OsteoMeasure System was used for data collection. The sampling site for the distal metaphysis was located 0.25–1.25 mm proximal to the growth plate. All bone histomorphometric data are reported using standard nomenclature (Dempster et al., 2013).

2.5 Biochemical markers of bone turnover

At the time of sacrifice, serum was collected via terminal bleeds from all mice as previously described (Hawse et al., 2014). ELISA kits (ImmunoDiagnostic Systems, Fountain Hills, AZ) for procollagen type 1 amino-terminal propeptide (P1NP) and C-Telopeptide of Type I Collagen (CTX-1) were used to assess circulating levels of these two proteins in the serum. All assays were performed in duplicate and averaged among the individual mouse groups.

2.6 Statistics

Results are expressed as mean ± SEM. Differences between genotypes (WT vs TIEG KO) and treatment (vehicle vs Scl-Ab) groups were examined by two-way ANOVA. If an interaction was not detected further analyses were performed to identify statistically significant differences between mouse genotypes and/or treatments. Significance was determined by $p<0.05$.

3. RESULTS

3.1 DXA and pQCT

As a first step in determining the effects of Scl-Ab treatment on the skeleton of WT and TIEG KO mice, we performed whole body DXA analyses (Table 1). This analysis revealed significant increases in whole body total bone mineral content and total bone mineral density with Scl-Ab treatment, irrespective of genotype.

As expected, pQCT analysis of the tibial metaphysis revealed significant decreases in metaphyseal total bone content, trabecular content, and trabecular area in vehicle treated TIEG KO mice compared to vehicle treated WT littermates (Table 1). At the tibial diaphysis, total bone content, cortical content, cortical area, periosteal circumference and endocortical circumference were also decreased in vehicle treated TIEG KO mice compared to WT

littermates. Treatment with Scl-Ab resulted in significant increases in tibial metaphysis total bone content, total density, and trabecular density as well as significant decreases in trabecular content and trabecular area, irrespective of mouse genotype (Table 1). At the tibial diaphysis, total content, total density, cortical content, cortical density and cortical were increased following Scl-Ab treatment, irrespective of mouse genotype (Table 1). Periosteal circumference was not significantly changed with treatment while endocortical circumference was decreased, irrespective of mouse genotype (Table 1).

3.2 MicroCT

We next performed μCT analysis of the femur. A representative image depicting the regions of interest in the femoral diaphysis (cortical bone), metaphysis (cancellous bone), and epiphysis (cancellous bone), and 3D reconstructions of one representative mouse femur from each group, are shown in Figure 1A.

At the femur diaphysis, a significant interaction between genotype and treatment was detected for marrow volume (Figure 1B). The decrease in marrow volume with Scl-Ab treatment was greater in WT than TIEG KO mice. Cross-sectional volume was significantly decreased in TIEG KO mice relative to WT controls (Figure 1B). Cortical thickness and cortical volume were significantly increased following Scl-Ab treatment in both WT and TIEG KO mice (Figure 1B).

Analysis of the femur metaphysis showed a significant interaction between genotype and treatment for trabecular number and trabecular spacing. Trabecular number increased and trabecular spacing decreased with Scl-Ab treatment in TIEG KO mice but not in WT mice (Figure 1C). A significant increase in bone volume/tissue volume and trabecular thickness was detected in response to Scl-Ab therapy irrespective of mouse genotype (Figure 1C).

At the distal femur epiphysis, there was no significant interaction between genotype and treatment for any of the parameters evaluated. However, significant decreases in bone volume/tissue volume, trabecular number and trabecular thickness, as well as a concomitant increase in trabecular spacing were detected in TIEG KO mice compared to WT littermates (Figure 1D). Similarly, bone volume/tissue volume, trabecular number and trabecular thickness were significantly increased following Scl-Ab treatment while trabecular spacing was significantly reduced (Figure 1D).

No significant interactions were detected between genotype and treatment for total femur bone volume and bone length (Table 2). However, bone volume was significantly increased in response to Scl-Ab therapy (Table 2).

MicroCT analysis of cancellous bone in the 3rd lumbar vertebra (Table 3) showed no significant interactions between genotype and treatment for any of the parameters evaluated. As with the femur, total bone volume was significantly increased in Scl-Ab treated mice relative to vehicle treated controls (Table 3). Connectivity density was significantly increased in TIEG KO mice relative to WT littermates (Table 3). Significant increases in bone volume/tissue volume, connectivity density, trabecular number and trabecular

thickness, as well as a concomitant decrease in trabecular spacing, were observed following Scl-Ab treatment (Table 3).

3.3 Histomorphometry

To identify changes at the cellular level in response to Scl-Ab treatment, we performed histomorphometric analysis of the distal femur metaphysis (Figure 2). This analysis revealed no significant interactions between genotype and treatment. However, significant increases in mineralizing perimeter/bone perimeter (M.Pm/B.Pm), mineral apposition rate (MAR), bone formation rate per bone area (BFR/B.Ar), BFR per tissue area (BFR/T.Ar) and BFR per bone perimeter (BFR/B.Pm) were noted with Scl-Ab treatment (Figure 2). Similarly, osteoblast perimeter/bone perimeter (Ob Pm/B.Pm) was significantly increased with Scl-Ab treatment (Figure 2). However, there were no significant changes in osteoclast perimeter/bone perimeter (Oc Pm/B.Pm) following Scl-Ab treatment (Figure 2).

3.4 Serum markers

In parallel to histomorphometry, we also analyzed a bone formation (P1NP) and a bone resorption (CTX-1) marker in the serum of all mice at the time of sacrifice. There was no significant interaction between genotype and treatment for P1NP and CTX-1 (Figure 3). Serum levels of P1NP were significantly higher in TIEG KO mice compared to WT littermates and were also elevated following Scl-Ab treatment (Figure 3). Circulating levels of CTX-1 were not significantly affected by mouse genotype or Scl-Ab treatment (Figure 3).

4. DISCUSSION

Given our previous findings demonstrating that deletion of TIEG results in increased sclerostin expression in bone (Subramaniam et al., 2018) and decreased Wnt signaling (Subramaniam et al., 2017a), we sought to determine if Scl-Ab therapy could rescue the low bone mass phenotype of TIEG KO mice. Our results demonstrate that Scl-Ab therapy has substantial bone beneficial effects on the mouse skeleton in WT and TIEG KO mice. Specifically, we found that Scl-Ab therapy for 6 weeks in TIEG KO and in WT controls significantly increased cortical and cancellous bone mass and improved bone microarchitecture. In the cortical bone of the femur, Scl-Ab treatment significantly increased cortical thickness, irrespective of genotype. Cross-sectional volume was not significantly changed with treatment. Marrow volume was found to decrease in a genotype and treatment specific manner, with marrow volume decreased to a greater extent in WT than in TIEG KO mice. Importantly, the trabecular bone compartment of the distal femur metaphysis and epiphysis showed significant increases in BV/TV and trabecular thickness following Scl-Ab treatment. Additionally there was a significant interaction between trabecular number and spacing in the metaphysis between genotype and treatment whereby Scl-Ab therapy had a larger effect in TIEG KO mice. Analysis of the vertebra also showed significant increases in bone volume, BV/TV, trabecular number and thickness, with concomitant reductions in trabecular spacing following Scl-Ab treatment.

Histomorphometic analyses showed significant increases in mineralizing bone perimeter and mineral apposition rate following Scl-Ab treatment, irrespective of genotype. Additionally,

measures of bone formation rate (BFR/B.Ar, BFR/T.Ar, and BFR/B.Pm) were all significantly increased with Scl-Ab treatment irrespective of genotype. At the biochemical level, a serum marker of bone formation (P1NP) was also significantly increased in Scl-Ab treated mice. Furthermore, osteoblast perimeter was significantly increased with Scl-Ab treatment in both genotypes. Interestingly, it has been reported that early responses to Scl-Ab therapy appear to directly activate bone lining cells thereby increasing osteoblast numbers (Boyce et al., 2017; Kim et al., 2017). This phase is followed by an attenuation of bone formation rates, but maintains a net positive bone formation with long-term treatment. Our work in the WT and TIEG KO animals showed similar responses including increased osteoblast perimeter and increased serum levels of P1NP. In contrast, clinical studies have revealed reductions in bone resorption markers in response to Scl-Ab therapy (McClung et al., 2014; Padhi et al., 2011). However, no significant effects of the Scl-Ab were observed on osteoclast perimeter or circulating levels of CTX-1 following 6 weeks of treatment in WT or TIEG KO mice. These discrepancies could be attributed to a species specific phenomenon as reports in female cynomolgus monkeys have also indicated no significant effects of Scl-Ab therapies on bone resorption (Ominsky et al., 2010). Furthermore, these differences could be explained by the time point chosen for analysis following Scl-Ab therapy in the present study given that indices of both bone formation and resorption have been shown to change during the course of therapy in humans (McClung et al., 2014; McColm et al., 2014; Padhi et al., 2011; Recker et al., 2015).

Post and peri-menopausal women have increased serum sclerostin levels as systemic estrogen levels decline (Clarke and Drake, 2013). Further, estrogen replacement therapy results in reduced circulating sclerostin (Modder et al.). Similarly, TIEG KO mice have elevated sclerostin levels (Subramaniam et al., 2018) and exhibit a female-specific low bone mass phenotype (Bensamoun et al., 2006a; Subramaniam et al., 2018), implicating the role of sex steroids in regulating bone mass in the TIEG KO mouse model. Previous work has demonstrated that TIEG expression is regulated by estrogen (Hawse et al., 2008b) and that loss of this gene attenuates the impact of OVX and estrogen replacement therapy (Hawse et al., 2014). The data presented here demonstrate that Scl-Ab treatment of female TIEG KO mice is capable of rescuing the osteopenic phenotype observed in these animals in spite of the known defects in the estrogen signaling pathway.

In summary, Scl-Ab treatment reversed most of the abnormalities associated with TIEG deficiency in the female mouse skeleton. Specifically, Scl-Ab treatment increased bone mass, improved cancellous microarchitecture and increased bone formation rates in both female WT and TIEG KO mice. Our results are in concordance with current clinical trials demonstrating the bone beneficial effects of this therapy for postmenopausal osteoporosis. Finally, these findings demonstrate that the efficacy of Scl-Ab therapy is independent of TIEG expression and/or function.

Acknowledgements

This work was supported by National Institutes of Health grants (DE14036 (JRH and MS)), T32AR056950 (AG) and F32AR49823 (AG), the Eisenberg Foundation and the Mayo Foundation. We would like to thank Amgen Inc (Thousand Oaks, CA, USA) and UCB (Brussels, Belgium) for the generous gift of the sclerostin antibody used in this study. We would also like to thank Dr. Thomas Spelsberg for his excellent mentorship and insightful comments.

References

Bensamoun SF, Hawse JR, Subramaniam M, Ilharreborde B, Bassillais A, Benhamou CL, Fraser DG, Oursler MJ, Amadio PC, An KN, Spelsberg TC. 2006a TGFbeta inducible early gene-1 knockout mice display defects in bone strength and microarchitecture. Bone 39(6):1244–1251. [PubMed: 16876494]

Bensamoun SF, Tsubone T, Subramaniam M, Hawse JR, Boumediene E, Spelsberg TC, An KN, Amadio PC. 2006b Age-dependent changes in the mechanical properties of tail tendons in TGF-beta inducible early gene-1 knockout mice. J Appl Physiol 101(5):1419–1424. [PubMed: 16794021]

Boyce RW, Niu QT, Ominsky MS. 2017 Kinetic reconstruction reveals time-dependent effects of romosozumab on bone formation and osteoblast function in vertebral cancellous and cortical bone in cynomolgus monkeys. Bone 101:77–87. [PubMed: 28428078]

Burgers TA, Williams BO. 2013 Regulation of Wnt/beta-catenin signaling within and from osteocytes. Bone 54(2):244–249. [PubMed: 23470835]

Canalis E 2013 Wnt signalling in osteoporosis: mechanisms and novel therapeutic approaches. Nat Rev Endocrinol 9(10):575–583. [PubMed: 23938284]

Cicek M, Vrabel A, Sturchio C, Pederson L, Hawse JR, Subramaniam M, Spelsberg TC, Oursler MJ. 2011 TGF-beta inducible early gene 1 regulates osteoclast differentiation and survival by mediating the NFATc1, AKT, and MEK/ERK signaling pathways. PloS one 6(3):e17522. [PubMed: 21423731]

Clarke BL, Drake MT. 2013 Clinical utility of serum sclerostin measurements. Bonekey Rep 2:361. [PubMed: 24578825]

Dallas SL, Prideaux M, Bonewald LF. 2013 The osteocyte: an endocrine cell … and more. Endocrine reviews 34(5):658–690. [PubMed: 23612223]

Dempster DW, Compston JE, Drezner MK, Glorieux FH, Kanis JA, Malluche H, Meunier PJ, Ott SM, Recker RR, Parfitt AM. 2013 Standardized nomenclature, symbols, and units for bone histomorphometry: a 2012 update of the report of the ASBMR Histomorphometry Nomenclature Committee. J Bone Miner Res 28(1):2–17. [PubMed: 23197339]

Hawse J, Iwaniec UT, Bensamoun SF, Monroe DG, Peters KD, Ilharreborde B, Rajamannan NM, Oursler MJ, Turner RT, Spelsberg TC, Subramaniam M 2008 TIEG-Null Mice Display an Osteopenic Gender-Specific Phenotype. . Bone.

Hawse JR, Cicek M, Grygo SB, Bruinsma ES, Rajamannan NM, van Wijnen AJ, Lian JB, Stein GS, Oursler MJ, Subramaniam M, Spelsberg TC. 2011 TIEG1/KLF10 modulates Runx2 expression and activity in osteoblasts. PLoS One 6(4):e19429. [PubMed: 21559363]

Hawse JR, Iwaniec UT, Bensamoun SF, Monroe DG, Peters KD, Ilharreborde B, Rajamannan NM, Oursler MJ, Turner RT, Spelsberg TC, Subramaniam M. 2008a TIEG-null mice display an osteopenic gender-specific phenotype. Bone 42(6):1025–1031. [PubMed: 18396127]

Hawse JR, Pitel KS, Cicek M, Philbrick KA, Gingery A, Peters KD, Syed FA, Ingle JN, Suman VJ, Iwaniec UT, Turner RT, Spelsberg TC, Subramaniam M. 2014 TGFbeta inducible early gene-1 plays an important role in mediating estrogen signaling in the skeleton. J Bone Miner Res 29(5):1206–1216. [PubMed: 24190163]

Hawse JR, Subramaniam M, Monroe DG, Hemmingsen AH, Ingle JN, Khosla S, Oursler MJ, Spelsberg TC. 2008b Estrogen receptor beta isoform-specific induction of transforming growth factor beta-inducible early gene-1 in human osteoblast cells: an essential role for the activation function 1 domain. Molecular endocrinology (Baltimore, Md 22(7):1579–1595.

Hoeppner LH, Secreto FJ, Westendorf JJ. 2009 Wnt signaling as a therapeutic target for bone diseases. Expert Opin Ther Targets 13(4):485–496. [PubMed: 19335070]

Hopwood B, Tsykin A, Findlay DM, Fazzalari NL. 2009 Gene expression profile of the bone microenvironment in human fragility fracture bone. Bone 44(1):87–101. [PubMed: 18840552]

Iwaniec UT, Wronski TJ, Turner RT. 2008 Histological analysis of bone. Methods in molecular biology (Clifton, NJ 447:325–341.

Kim SW, Lu Y, Williams EA, Lai F, Lee JY, Enishi T, Balani DH, Ominsky MS, Ke HZ, Kronenberg HM, Wein MN. 2017 Sclerostin Antibody Administration Converts Bone Lining Cells Into Active Osteoblasts. J Bone Miner Res 32(5):892–901. [PubMed: 27862326]

Lee B, Iwaniec UT, Turner RT, Lin YW, Clarke BL, Gingery A, Wei LN. 2017 RIP140 in monocytes/macrophages regulates osteoclast differentiation and bone homeostasis. JCI Insight 2(7):e90517. [PubMed: 28405613]

Leupin O, Piters E, Halleux C, Hu S, Kramer I, Morvan F, Bouwmeester T, Schirle M, Bueno-Lozano M, Fuentes FJ, Itin PH, Boudin E, de Freitas F, Jennes K, Brannetti B, Charara N, Ebersbach H, Geisse S, Lu CX, Bauer A, Van Hul W, Kneissel M. 2011 Bone overgrowth-associated mutations in the LRP4 gene impair sclerostin facilitator function. The Journal of biological chemistry 286(22):19489–19500. [PubMed: 21471202]

Li X, Zhang Y, Kang H, Liu W, Liu P, Zhang J, Harris SE, Wu D. 2005 Sclerostin binds to LRP5/6 and antagonizes canonical Wnt signaling. The Journal of biological chemistry 280(20):19883–19887. [PubMed: 15778503]

McClung MR, Grauer A, Boonen S, Bolognese MA, Brown JP, Diez-Perez A, Langdahl BL, Reginster JY, Zanchetta JR, Wasserman SM, Katz L, Maddox J, Yang YC, Libanati C, Bone HG. 2014 Romosozumab in postmenopausal women with low bone mineral density. N Engl J Med 370(5):412–420. [PubMed: 24382002]

McColm J, Hu L, Womack T, Tang CC, Chiang AY. 2014 Single- and multiple-dose randomized studies of blosozumab, a monoclonal antibody against sclerostin, in healthy postmenopausal women. J Bone Miner Res 29(4):935–943. [PubMed: 23996473]

Modder UI, Clowes JA, Hoey K, Peterson JM, McCready L, Oursler MJ, Riggs BL, Khosla S. Regulation of circulating sclerostin levels by sex steroids in women and in men. J Bone Miner Res 26(1):27–34. [PubMed: 20499362]

Modder UI, Hoey KA, Amin S, McCready LK, Achenbach SJ, Riggs BL, Melton LJ, 3rd, Khosla S. 2011 Relation of age, gender, and bone mass to circulating sclerostin levels in women and men. J Bone Miner Res 26(2):373–379. [PubMed: 20721932]

Ominsky MS, Boyce RW, Li X, Ke HZ. 2017 Effects of sclerostin antibodies in animal models of osteoporosis. Bone 96:63–75. [PubMed: 27789417]

Ominsky MS, Vlasseros F, Jolette J, Smith SY, Stouch B, Doellgast G, Gong J, Gao Y, Cao J, Graham K, Tipton B, Cai J, Deshpande R, Zhou L, Hale MD, Lightwood DJ, Henry AJ, Popplewell AG, Moore AR, Robinson MK, Lacey DL, Simonet WS, Paszty C. 2010 Two doses of sclerostin antibody in cynomolgus monkeys increases bone formation, bone mineral density, and bone strength. J Bone Miner Res 25(5):948–959. [PubMed: 20200929]

Padhi D, Jang G, Stouch B, Fang L, Posvar E. 2011 Single-dose, placebo-controlled, randomized study of AMG 785, a sclerostin monoclonal antibody. J Bone Miner Res 26(1):19–26. [PubMed: 20593411]

Philbrick KA, Turner RT, Branscum AJ, Wong CP, Iwaniec UT. 2015 Paradoxical effects of partial leptin deficiency on bone in growing female mice. Anat Rec (Hoboken) 298(12):2018–2029. [PubMed: 26370912]

Recker RR, Benson CT, Matsumoto T, Bolognese MA, Robins DA, Alam J, Chiang AY, Hu L, Krege JH, Sowa H, Mitlak BH, Myers SL. 2015 A randomized, double-blind phase 2 clinical trial of blosozumab, a sclerostin antibody, in postmenopausal women with low bone mineral density. J Bone Miner Res 30(2):216–224. [PubMed: 25196993]

Reinholz MM, An MW, Johnsen SA, Subramaniam M, Suman VJ, Ingle JN, Roche PC, Spelsberg TC. 2004 Differential gene expression of TGF beta inducible early gene (TIEG), Smad7, Smad2 and Bard1 in normal and malignant breast tissue. Breast Cancer Res Treat 86(1):75–88. [PubMed: 15218362]

Robling AG, Niziolek PJ, Baldridge LA, Condon KW, Allen MR, Alam I, Mantila SM, Gluhak-Heinrich J, Bellido TM, Harris SE, Turner CH. 2008 Mechanical stimulation of bone in vivo reduces osteocyte expression of Sost/sclerostin. The Journal of biological chemistry 283(9):5866–5875. [PubMed: 18089564]

Subramaniam M, Cicek M, Pitel KS, Bruinsma ES, Nelson Holte MH, Withers SG, Rajamannan NM, Secreto FJ, Venuprasad K, Hawse JR. 2017a TIEG1 modulates beta-catenin sub-cellular localization and enhances Wnt signaling in bone. Nucleic acids research 45(9):5170–5182. [PubMed: 28201653]

Subramaniam M, Cicek M, Pitel KS, Bruinsma ES, Nelson Holte MH, Withers SG, Rajamannan NM, Secreto FJ, Venuprasad K, Hawse JR. 2017b TIEG1 modulates beta-catenin sub-cellular localization and enhances Wnt signaling in bone. Nucleic Acids Res.

Subramaniam M, Gorny G, Johnsen SA, Monroe DG, Evans GL, Fraser DG, Rickard DJ, Rasmussen K, van Deursen JM, Turner RT, Oursler MJ, Spelsberg TC. 2005 TIEG1 null mouse-derived osteoblasts are defective in mineralization and in support of osteoclast differentiation in vitro. Mol Cell Biol 25(3):1191–1199. [PubMed: 15657444]

Subramaniam M, Harris SA, Oursler MJ, Rasmussen K, Riggs BL, Spelsberg TC. 1995 Identification of a novel TGF-beta-regulated gene encoding a putative zinc finger protein in human osteoblasts. Nucleic Acids Res 23(23):4907–4912. [PubMed: 8532536]

Subramaniam M, Pitel KS, Bruinsma ES, Monroe DG, Hawse JR. 2018 TIEG and estrogen modulate SOST expression in the murine skeleton. J Cell Physiol 233(4):3540–3551. [PubMed: 29044507]

Subramaniam M, Pitel KS, Withers SG, Drissi H, Hawse JR. 2016 TIEG1 enhances Osterix expression and mediates its induction by TGFbeta and BMP2 in osteoblasts. Biochemical and biophysical research communications 470(3):528–533. [PubMed: 26801561]

Yerges LM, Klei L, Cauley JA, Roeder K, Kammerer CM, Ensrud KE, Nestlerode CS, Lewis C, Lang TF, Barrett-Connor E, Moffett SP, Hoffman AR, Ferrell RE, Orwoll ES, Zmuda JM. 2010 Candidate gene analysis of femoral neck trabecular and cortical volumetric bone mineral density in older men. J Bone Miner Res 25(2):330–338. [PubMed: 19619005]

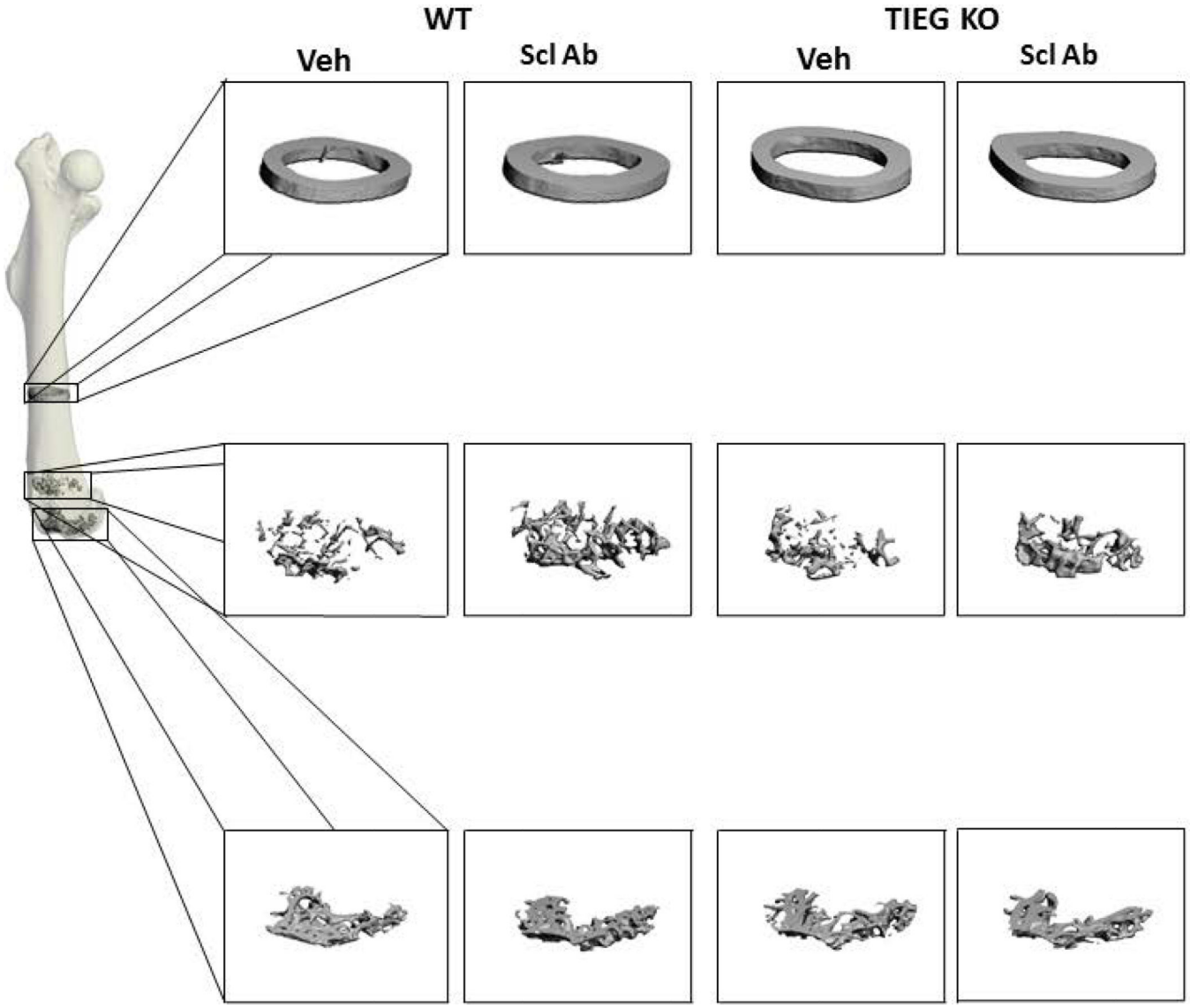

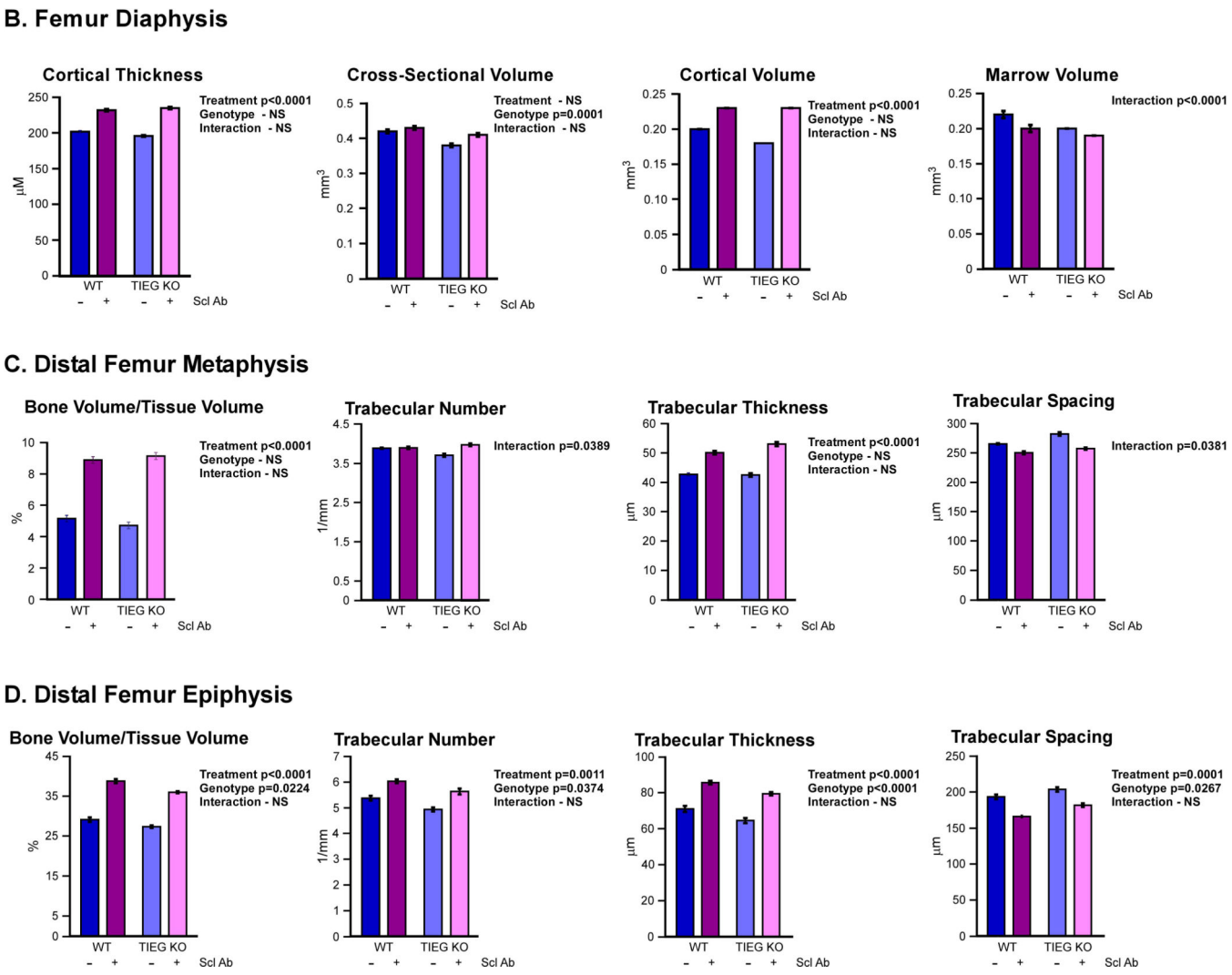

Figure 1.

MicroCT analysis of WT and TIEG KO mouse femurs following vehicle and Scl-Ab treatment. A. Representative images of µCT reconstruction at the femur diaphysis, metaphysis and epiphysis of a single mouse from each treatment group. Indicated parameters were analyzed at the femur diaphysis (B), distal femur metaphysis (C) and distal femur epiphysis (D) following 6 weeks of vehicle or Scl-Ab treatment of WT and TIEG KO female mice. Data shown are representative of 12 mice per group. P values for assessing differential response to treatment as a function of genotype are indicated by an interaction term. If no interaction was detected, p values are shown for comparisons between mouse genotypes and mouse treatments.

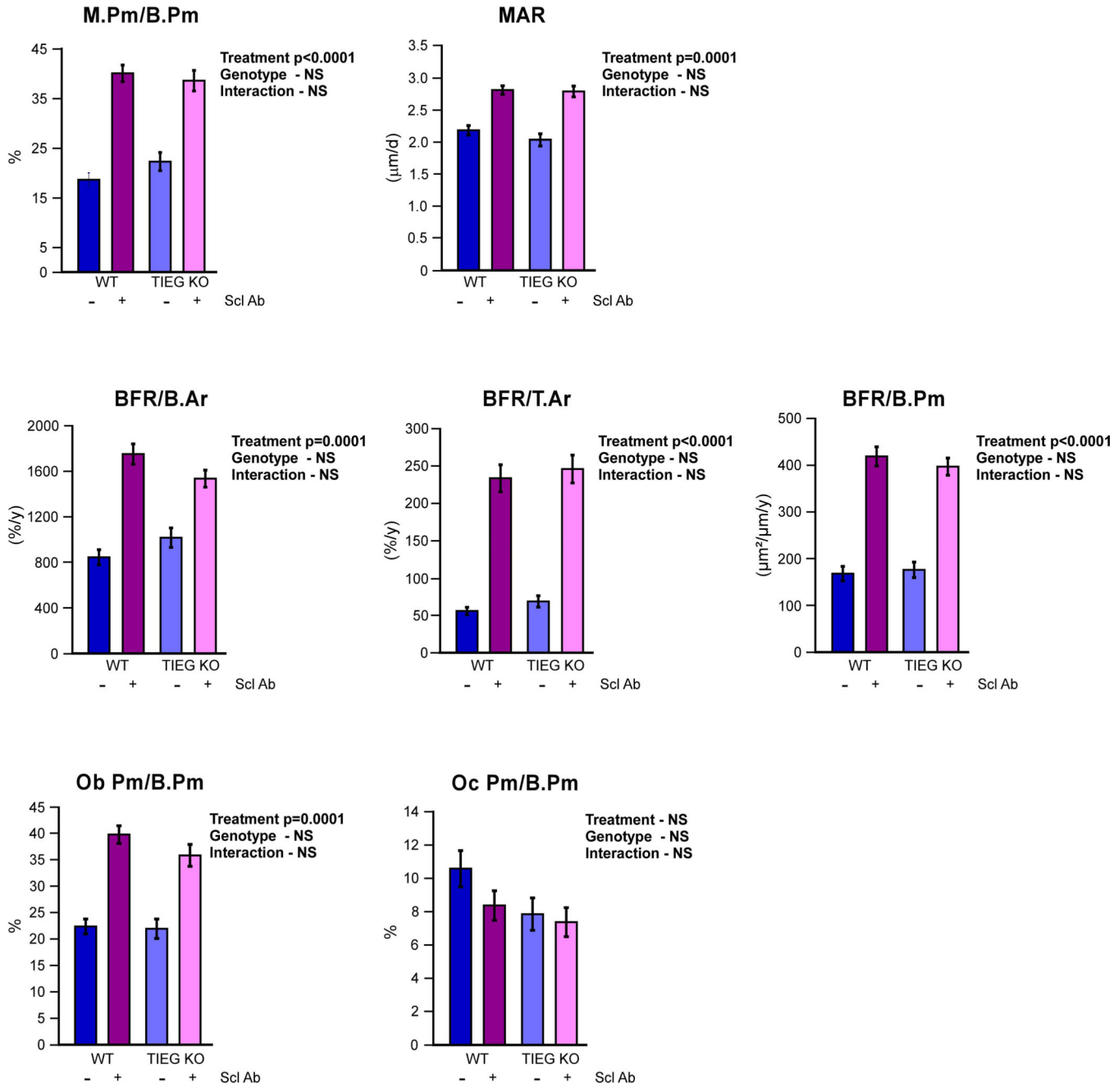

Figure 2.

Histomorphometric analysis of WT and TIEG KO mouse femurs following vehicle and Scl-Ab treatment. Indicated parameters were analyzed following 6 weeks of vehicle or Scl-Ab treatment of WT and TIEG KO female mice. Data shown are representative of 12 mice per group. P values for assessing differential response to treatment as a function of genotype are indicated by an interaction term. If no interaction was detected, p values are shown for comparisons between mouse genotypes and mouse treatments.

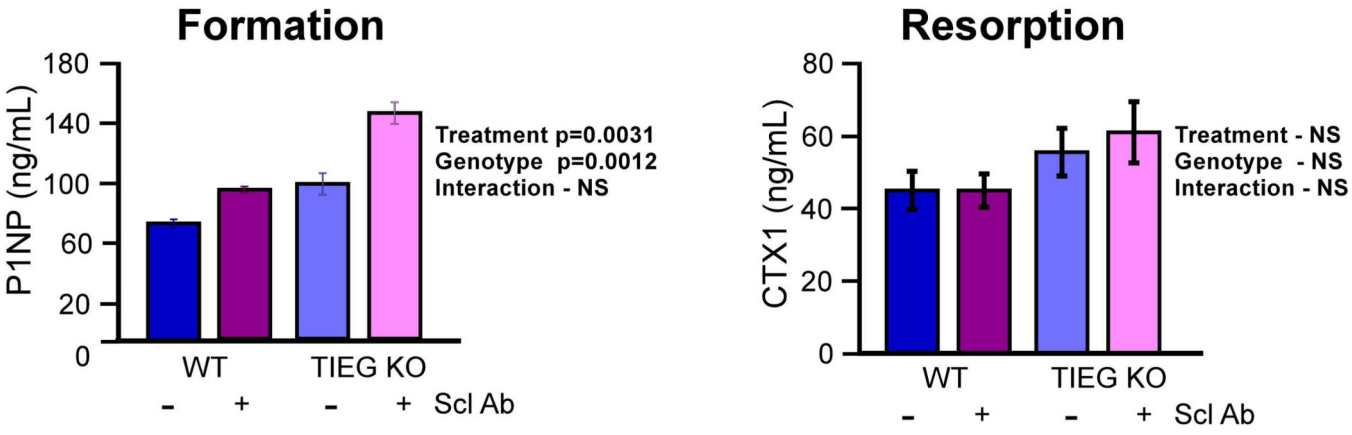

Figure 3.

Assessment of bone formation and resorption markers. Serum levels of P1NP and CTX-1 were determined in WT and TIEG KO female mice following 6 weeks of treatment with vehicle (−) or Scl-Ab (+). Data shown are representative of 12 mice per group. P values for assessing differential response to treatment as a function of genotype are indicated by an interaction term. If no interaction was detected, p values are shown for comparisons between mouse genotypes and mouse treatments.

Table 1.

DXA and pQCT analysis of Scl Ab treatment

DXA Whole Body Analysis	WT Veh (n = 11)	WT Scl Ab (n = 12)	TIEG KO Veh (n = 12)	TIEG KO Scl Ab (n = 12)	Treatment	Model	Interaction
Total Bone Mineral Density (g/cm^2)	0.057 ± 0.002	0.063 ± 0.001	0.057 ± 0.002	0.060 ± 0.001	0.0041	NS	NS
Total Bone Mineral Content (g)	0.476 ± 0.019	0.550 ± 0.017	0.456 ± 0.020	0.506 ± 0.012	0.0005	NS	NS
pQCT Tibial Metaphysis Analysis							
Total Content (mg)	1.45 ± 0.03	1.67 ± 0.04	1.37 ± 0.03	1.62 ± 0.02	<0.0001	0.0266	NS
Total Density (mg/cm^3)	426 ± 9	500 ± 7	430 ± 6	506 ± 7	<0.0001	NS	NS
Trabecular Content (mg)	0.279 ± 0.008	0.239 ± 0.011	0.239 ± 0.011	0.230 ± 0.012	0.0105	0.0105	NS
Trabecular Density (mg/cm^3)	201 ± 3	208 ± 4	190 ± 4	207 ± 4	NS	0.0054	NS
Trabecular Area (mm^2)	1.40 ± 0.05	1.16 ± 0.04	1.25 ± 0.04	1.11 ± 0.04	0.0001	0.0334	NS
pQCT Tibial Diaphysis Analysis							
Total Content (mg)	1.01 ± 0.03	1.13 ± 0.03	0.92 ± 0.01	1.06 ± 0.01	<0.0001	0.0002	NS
Total Density (mg/cm^3)	734 ± 6	799 ± 7	736 ± 7	813 ± 7	NS	<0.0001	NS
Cortical Content (mg)	0.785 ± 0.020	0.906 ± 0.022	0.708 ± 0.014	0.853 ± 0.011	<0.0001	0.0005	NS
Cortical Density (mg/cm^3)	1129 ± 5	1177 ± 5	1120 ± 5	1176 ± 4	<0.0001	NS	NS
Cortical Area (mm^2)	0.696 ± 0.017	0.770 ± 0.017	0.631 ± 0.011	0.723 ± 0.009	<0.0001	0.0002	NS
Cortical Thickness (mm)	0.362 ± 0.009 (n=3)	0.404 ± 0.007 (n=8)	0.365 ± 0.004 (n=6)	0.401 ± 0.009 (n=7)	NS	NS	NS
Periosteal Circumference (mm)	4.16 ± 0.05	4.21 ± 0.05	3.96 ± 0.03	4.04 ± 0.03	NS	<0.0001	NS
Endosteal Circumference (mm)	2.93 ± 0.04	2.83 ± 0.04	2.78 ± 0.03	2.69 ± 0.03	<0.0001	<0.0001	<0.0001

Data expressed as mean ± SE. Two-way ANOVA reported as interaction. Significance in ANOVA for treatment or model are noted. Significance level $p \leq 0.05$.

Table 2.

Total Femur analysis

Total Femur	WT Veh (n = 10)	WT Scl Ab (n = 11)	TIEG KO Veh (n = 8)	TIEG KO Scl Ab (n = 10)	Treatment	Model	Interaction
Bone Volume (mm^3)	19.24 ± 0.34	22.21 ± 0.52	17.67 ± 0.38	22.21 ± 0.52	0.0391	0.0713	0.5155
Bone Length (mm)	15.6 ± 0.01	15.4 ± 0.01	15.2 ± 0.1	15.2 ± 0.1	0.6911	0.1302	0.6911

Data expressed as mean ± SE.

Table 3.

MicroCT analysis of L3 Vertebra in mice following 6 weeks of vehicle (Veh) or sclerostin antibody (Scl Ab) treatment

Vertebra	WT Veh (n = 11)	TIEG KO Veh (n = 12)	WT Scl Ab (n = 12)	TIEG KO Scl Ab (n = 12)	Treatment	Model	Interaction
Bone volume (mm3)	4.81 ± 0.14	4.65 ± 0.16	6.05 ± 0.16	6.14 ± 0.09	<0.0001	0.6735	0.3882
3rd Lumbar vertebra							
Bone Volume/Total Volume (%)	12.38 ± 0.34	12.69 ± 0.86	20.28 ± 0.86	21.04 ± 0.6	<0.0001	0.5994	0.5155
Connectivity Density ($1/mm^3$)	130.76 ± 7.17	158.65 ± 15.69	151.35 ± 8.38	184.31 ± 8.45	0.0395	0.0071	0.5745
Trabecular Number (1/mm)	3.66 ± 0.06	3.85 ± 0.16	4.11 ± 0.12	4.17 ± 0.07	0.0011	0.3001	0.4747
Trabecular Thickness (μm)	41 ± 1	40 ± 1	53 ± 1	52 ± 1	<0.0001	0.1625	1
Trabecular Spacing (μm)	276 ± 5	268 ± 11	246 ± 8	241 ± 4	0.0004	0.4245	0.657

Data expressed as mean ± SE.